Optimization of guided wave array for inspection of large plate structures

Alexander Velichko

Citation: AIP Conference Proceedings **1706**, 030005 (2016); doi: 10.1063/1.4940477
View online: http://dx.doi.org/10.1063/1.4940477
View Table of Contents: http://scitation.aip.org/content/aip/proceeding/aipcp/1706?ver=pdfcov
Published by the AIP Publishing

Optimization of Guided Wave Array for Inspection of Large Plate Structures

Alexander Velichko

Department of Mechanical Engineering, University of Bristol, Bristol, BS8 1TR, UK

Corresponding author: a.velichko@bristol.ac.uk

Abstract. The paper describes a general approach for processing data from a guided wave transducer array on a plate-like structure. The problem of finding optimal array element layout, which allows the number of elements and amount of measured data to be minimized without compromising array performance, is considered. It is shown that in the case of the far field imaging the image can be reconstructed using much fewer array elements than the classical Nyquist–Shannon sampling theorem requires. A new sampling criterion is derived and an optimised sparse array layout is proposed. The theory is validated experimentally using a guided wave array containing electromagnetic acoustic transducer elements for exciting and detecting the S_0 Lamb wave mode in a 3-mm-thick aluminum plate.

INTRODUCTION

Ultrasonic guided waves are widely used in many areas of nondestructive evaluation [1]. In this paper the problem of synthesizing an image of a plate-like structure with a guided wave transducer array is considered. It is assumed that the transmitter and receiver elements are located at the points $\mathbf{r}_{(T)i}$ and $\mathbf{r}_{(R)j}$, respectively, and that the coordinate origin is the centre of the array. The complete raw data set of signals from every transmitter-receiver combination, s_{ij}, is collected and then post-processed. For a 2D array, where array elements are located in some area of a 2-dimensional plane (array aperture), there is an infinite number of possible array element configurations. In this case the fundamental problem is to find an optimal array element layout and corresponding data processing method in order to obtain the high resolution image with minimum number of array elements.

The general imaging approach is to multiply the transmitted and received signals by suitable amplitude and phase factors and add them together in order to focus the beam on every point within the test structure. The algorithms differ in the way in which these coefficients are calculated. The imaging algorithms transform the array data into an image, which indicates the location of the defects in the sample. According to the distance between an array and the testing area it is possible to distinguish between two cases: near field imaging and far field imaging.

In practice the near field of the array can be approximately estimated as:

$$r < D^2 / \lambda , \tag{1}$$

where r is the distance between reflector and the array, D is the linear size of the array aperture and λ is wavelength. In this case the reflector can be seen by the array from different angles and advanced methods for reflector characterization can be applied.

The further a reflector is from an array, the smaller the range of angles it is illuminated over. If the distance between the array and reflector satisfies the following condition

$$r > D^2 / \lambda , \tag{2}$$

it is possible to consider that the reflector is seen by the array from approximately from one angle only. In the far field focusing is not possible and the imaging methods only have the effect of beam steering.

The array data s_{ij} represent samples of the continuous transmitted and received wavefield $s(\mathbf{r}_{(T)},\mathbf{r}_{(R)})$, so $s_{ij}= s(\mathbf{r}_{(T)i},\mathbf{r}_{(R)j})$. The best performance of the array can be achieved if the function $s(\mathbf{r}_{(T)},\mathbf{r}_{(R)})$ can be reconstructed from its sample values s_{ij} , otherwise there is loss of information. If the reflector is in the near-field of the array then the function s is an arbitrary bandlimited function. In this case in order to preserve the information which could be

42nd Annual Review of Progress in Quantitative Nondestructive Evaluation
AIP Conf. Proc. 1706, 030005-1–030005-9; doi: 10.1063/1.4940477

collected by an array, the array aperture must be fully populated with array elements using some sampling scheme. Any sampling pattern has corresponding sampling criterion. If the distance between sampling points is greater than some maximum allowable value then high-frequency components of the function *s* appear as low-frequency components of the reconstructed function. This effect is called aliasing. For example, the spacing between sampling points in rectangular pattern must be less than $\lambda/2$.

In the far-field of the array the frequency spectrum of transmitter-receiver signal can be written as [2-4]

$$s_{ij} \sim \exp\left(-ik\left(\mathbf{r}_{(T)i} + \mathbf{r}_{(R)j}\right)\mathbf{n}\right)\exp\left(i2kr\right), \tag{3}$$

where $\mathbf{n}=\mathbf{r}/r$ is a unit vector pointing from the array to the reflector, $k=2\pi/\lambda$ is the wavenumber and the polar coordinate system (r, φ), where r and φ represent, respectively, radial and angular position, is defined with its origin at the nominal centre of the array. Therefore in the far field the processing algorithm can be divided into two parts [3,4]. The first part is the extraction of a reflected signal from the array data for each azimuthal direction, φ, and is associated with angular resolution. The second part is the mapping of extracted signal for each direction to the radial distance r. This step is associated with radial resolution.

The expression (3) shows that the function *s* depends only on one variable $\mathbf{r}_{(T)}+\mathbf{r}_{®}$ and can be written as

$$s_m \sim \exp\left(-ik\mathbf{r}_m\mathbf{n}\right),\ \mathbf{r}_m = \mathbf{r}_{(T)i} + \mathbf{r}_{(R)j}\,. \tag{4}$$

The expression (4) shows that in the far-field the transmitter-receiver array data is equivalent to the array of receivers located at the points $\mathbf{r}_m$ with one transmitter at the origin [2,3]. This effective receiver array is called a coarray [2] or effective aperture [3]. Note that each element in effective aperture represents contribution from one transmit-receive signal in original data. For example, for a rectangular array with elements around the perimeter that act as transmitters and receivers, the equivalent receiver array is a rectangular matrix array with an aperture of twice the size that is fully populated with elements. For a circular array with transducers around the perimeter only, the equivalent receiver array consists of a circular area of twice the diameter densely populated with elements. Generally, for a fully populated transmitter-receiver array the corresponding effective array is the same as for a sparse array with the elements located along the perimeter of the original array. The very important conclusion from this analysis is that in the far field there is a significant redundancy in the fully populated transmitter-receiver array data and performance of fully populated array can be achieved by using sparse array [2-4].

Based on this principle several guided wave array prototypes [5,6] and different signal processing methods have been developed [3,4]. However, the problem of optimal inter-element spacing in a sparse array hasn't been fully investigated. Numerical calculations performed in [5] showed that there is no precise relationship between maximum inter-element spacing and the appearance of grating lobes in the image, but in order to avoid the appearance of grating lobes the maximum element spacing must be approximately equal to $\lambda/3$. Note, that in this case the specific array geometry (circular array) and imaging technique (phased addition method) were used. Therefore it is uncertain if this sampling criterion is a fundamental array property or just related to the specific array geometry and processing method.

The one-third of the wavelength sampling rule has a major impact on the design of the physical array. For example, in [5] electro-magnetic acoustic transducers (EMAT) were used to generate and detect S_0 Lamb wave mode. However, the optimal EMAT size needs to be of the order of two-thirds of a wavelength in order to maximize the sensitivity to the S0 mode [5]. These two conflicting requirements mean that the transducers must be placed with overlapping, which makes the whole array construction significantly more complicated.

In this paper the image reconstruction from the guided wave array data is performed by rigorously solving the inverse imaging problem. The sampling criterion is analyzed and it is shown that the one-third of the wavelength requirement can be significantly relaxed without image degradation. Based on the established sampling rule the novel guided wave EMAT array layout is suggested, which allows to place transducer elements without overlapping. Finally, the array prototype has been constructed and tested on a 3-mm thick aluminum plate with multiple artificial defects.

FORMULATION OF INVERSE PROBLEM

In the previous section it has been shown that in the far field the imaging algorithm can be divided into two parts, angular resolution and radial resolution. The radial resolution represents a one-dimensional mapping of a guided wave signal from time to radial distance and can be performed using well established dispersion compensation

technique [7]. In this section the angular resolution problem is formulated as an inverse problem and the solution procedure is proposed.

From an array point of view each reflector located in the far field is characterised by a reflection coefficient. Arbitrary distribution of reflectors is described by the density distribution of reflection coefficient, $C(\varphi, \omega)$, where ω is the circular frequency. Because the angular resolution is performed at each frequency independently, below the dependence of the function C on the frequency will be omitted. The measured transmitter-receiver signal is a superposition of responses from reflectors located in all directions. Using expression (4) the array data in the effective aperture domain can be written as an integral over the azimuthal angle φ as

$$s(\mathbf{r}_{ef}) = \int_0^{2\pi} C(\varphi) \exp(-ik\mathbf{r}_{ef}\mathbf{n}) d\varphi \,. \tag{5}$$

The imaging problem consists of reconstructing the function $C(\varphi)$ from a set of measurements $s_m = s(\mathbf{r}_m)$. One possible solution is to discretize the unknown function $C(\varphi) = \{C(\varphi_1), \ldots C(\varphi_n)\}$, $n \le m$, then approximate the integral in (5) by some quadrature rule and, finally, solve the resulting system of linear equations. In this paper an alternative approach is used which allows to get an estimation of the minimum number of measurements required for the reconstruction of the reflectivity function $C(\varphi)$.

The function $C(\varphi)$ can be decomposed into Fourier series as

$$C(\varphi) = \frac{1}{2\pi} \sum_{n=-\infty}^{+\infty} C_n e^{in\varphi} \,. \tag{6}$$

By substituting this expression into equation (5) and calculating integrals the following equation can be obtained:

$$s(\mathbf{r}_{ef}) = 2\pi \sum_{n=-\infty}^{+\infty} C_n (-i)^n J_n(kr_{ef}) e^{in\varphi_{ef}} \,, \tag{7}$$

where (r_{ef}, φ_{ef}) are the polar coordinates in the effective aperture domain and J_n is the Bessel function of the first kind. For large orders n the Bessel function has the following asymptotic form:

$$J_n(z) \sim \frac{1}{\sqrt{2\pi n}} \left(\frac{ez}{2n} \right)^n \,, \; n \to \infty \,. \tag{8}$$

The asymptotic expression (8) shows that only a limited number of Fourier coefficients C_n, $n \le N$, contribute into the measurements $s(\mathbf{r}_{ef})$. Therefore, the minimum number of required transmitter-receiver measurements, or sampling points in the effective array domain, is given by

$$N_{ef,\min} \sim \frac{2\pi e \max(r_{ef})}{\lambda} \,. \tag{9}$$

For a finite set of transmitter-receiver signals $s_m = s(\mathbf{r}_m)$, $m \ge N_{ef}$, equation (7) represents an overdetermined system of linear equations. Finally, Fourier coefficients C_n, $n \le N_{ef}$, can be reconstructed by solving this system using regularization methods.

EFFECTIVE ARRAY OPTIMIZATION

Equation (5) leads to the very important conclusion: in the far-field image reconstruction depends on the sampling in the effective array domain only. Moreover, the structure of equation (7) in the form of Fourier series suggests that the main parameter of effective array which affects the angular resolution is the angular spacing between effective array elements. From (9) the following criterion for the angular sampling can be derived:

$$\Delta\varphi_{ef} \le \frac{2\pi}{N_{ef}} = \frac{\lambda}{e \max(r_{ef})} \,. \tag{10}$$

For example, the simplest possible effective array configuration which satisfies (10) is a ring with the radius $\max(r_{ef})$ and angular spacing between sampling points given by (10). However, if the argument of Bessel function is fixed then the Bessel function as a function of its order *n* has an oscillatory behaviour. It means that some terms in the series (7) might be very small and it will be impossible to reconstruct corresponding Fourier coefficients C_n. This situation is illustrated in Fig.1 which shows the angular resolution for the point reflector $C(\varphi) = \delta(\varphi - \pi)$, $C_n = 1$. The effective array consists of a single ring of 48 elements, the radius of the ring is 0.1 m, the wavelength is 35 mm and the angular spacing corresponds to the criterion (10). It can be seen that because of the effective array geometry grating lobes appear in the image. On the other hand, Fig.2 shows the reconstruction of the same function when the radial coordinates of the sampling points in the effective array domain are different, but the angular spacing still satisfies to condition (10). In this case in can be seen that all grating lobes are significantly suppressed.

Note that the previous analysis is performed in the single-frequency case. In order to achieve good angular resolution at multiple frequencies more variation in the radial coordinates of the effective array elements than shown in Fig.2 is required. Therefore, it is possible to conclude that the optimal distribution of effective array elements has to be uniform in the effective array aperture in both angular and radial directions, with the average angular spacing given by the condition (10).

(a) (b)

FIGURE 1. (a) Single ring effective array geometry; (b) the corresponding Point Spread Function.

(a) (b)

FIGURE 2. (a) Effective array geometry with elements at different radial distances; (b) the corresponding Point Spread Function.

PHYSICAL ARRAY OPTIMIZATION

The main challenge in finding the optimal physical array layout is due to the fact that there is no one-to-one relationship between element distributions in effective and physical array domains. Therefore, generally it is not possible to find a physical array element distribution which gives some predefined effective elements distribution. However, the analysis of the optimal sampling in the effective array domain allows to estimate the minimum number of required physical array elements. It is assumed that each array element can act as transmitter and receiver and the array elements are contained in the circle of diameter *D*. The last condition follows from the requirement for the physical array to be omnidirectional. If the total number of array elements is *N*, then the number of different

transmitter-receiver combinations is $N_{ef} = N(N-1)/2 \approx N^2/2$. The effective aperture represents a circle of twice the diameter of the physical array, $\max(r_{ef}) = D$. Then from the expression (9) it follows that the minimum number of array elements is given by

$$N_{\min} \sim 2\sqrt{\frac{e\pi D}{\lambda}}. \tag{11}$$

Firstly, the case of single circular ring of elements with the diameter D and angular interval $\Delta\varphi_{ring}$ is considered. Then the coordinates of the m-th effective array element corresponding to the vector sum of physical array elements i and j can be written as

$$x_{ef,m} = R_{ef,m}\cos\left(\frac{\Delta\varphi_{ring}}{2}(i+j)\right),\ R_{ef,m} = D\cos\left(\frac{\Delta\varphi_{ring}}{2}(i-j)\right). \tag{12}$$

It can be see that the angular sampling in the effective array domain is given by $\Delta\varphi_{ef} = 0.5\Delta\varphi_{ring}$. From the sampling condition (10) it follows that angular interval $\Delta\varphi_{ring}$ must satisfy to the following requirement

$$\Delta\varphi_{ring} \le \frac{2\lambda}{eD}. \tag{13}$$

Note that condition (13) corresponds to the inter-element distance

$$d_{ring} \approx \frac{1}{2}D\Delta\varphi_{ring} \le \frac{\lambda}{e}. \tag{14}$$

This relationship agrees with one-third of the wavelength criterion empirically obtained in [5]. Using relationships (9) and (11) the number of elements required in the ring array can be estimated as

$$N_{ring} = \frac{1}{2}N_{ef,\min} \approx \frac{1}{4}N_{\min}^2. \tag{15}$$

Therefore, a single ring array layout is not optimal for the far-field imaging. Firstly, the inter-element spacing requirement is too restrictive and, secondly, as it will be shown later, the number of array elements can be reduced.

The angular sampling condition (13) for the ring array is caused by the regularity of the physical array layout. As a result multiple elements in the effective array domain have the same angular coordinate (see expression (12)), and, consequently, more elements in the physical array domain are required in order to satisfy sampling condition (13). An alternative option is to use irregular distribution of the array elements. One of the best solutions is a Poisson disk distribution – random element locations with constraint on minimum separation distance [8]. In this case the effective array elements are also distributed randomly. It is supposed that at least for some "optimal" random array configurations the corresponding effective array elements are not crusted together and, therefore, the optimal number of physical array elements can be assumed to satisfy expression (11).

The goal of array optimization is to find an array layout with minimum number of elements which satisfies to the sampling criterion (10) and would not require the transducer coils to be overlapped. The optimal inter-element distance in the physical array can be estimated as $d \approx D/\sqrt{N_{\min}}$. Using expression (11) the following relationship can be obtained

$$d \approx \left[\frac{D^3\lambda}{4\pi e}\right]^{1/4}. \tag{16}$$

The experimental testing was performed using EMAT elements designed to excite and detect the S_0 Lamb wave mode and have equal transmission and reception sensitivity in all directions [4, 5]. The EMAT consists of 28-mm diameter pancake coil and the array was used on a 3-mm-thick aluminum plate specimen. Previously it has been shown that the EMAT has the highest sensitivity when the coil size is approximately equal to $2/3\lambda$ [5]. The phase velocity of the S_0 mode is approximately constant at low frequencies and for the considered plate is 5330 m/s. Therefore, the optimal performance of the EMAT corresponds to the wavelength $\lambda \approx 40$ mm at approximately 130

kHz. The array layout without overlapping EMATs is possible if the inter-element spacing is greater than the EMAT size, $d_{rand} \geq 2/3\lambda$, or

$$D \geq \left[\frac{64}{81}\pi e\right]^{1/3} \lambda \approx 1.9\lambda . \tag{17}$$

Assuming λ=40 mm the estimate for the array size is D≥76 mm. Based on the above analysis the following array optimization procedure has been used. Firstly, multiple random array configurations with the array aperture from 80 mm to 160 mm were generated with the minimum element spacing equal to 32 mm. This element spacing is slightly greater than the EMAT coil diameter and accounts for the magnets of 30 mm diameter with 2 mm spacing between them. Then transmitter-receiver data was simulated for each array layout for the case of the point reflector located at different angular directions at the distance of 0.33m from the array centre. Although the theory is developed for the far field imaging, the finite distance from the reflector to the array was chosen in order include near-field effects during the optimization process. The transmitted signal used was a 3 cycle Hanning windowed toneburst with a centre frequency of 150 kHz. The images were generated using the inversion algorithm described in the previous section. The Signal-to-Noise Ratio (SNR) was chosen as a quantitative metric of the image quality. The noise was calculated as a maximum image amplitude outside the ±20˚ angular interval around the main lobe. Note, that the described process of array optimization was mainly used as a proof of concept for the far field imaging theory. In principle, more rigorous optimization procedure can be applied, which potentially can further improve the imaging performance.

The best array performance was achieved by 138 mm diameter array with 17 elements. The array geometry and the corresponding effective array are shown in Fig. 3. Note that expression (11) with λ=36 mm gives N_{min}=12 for the minimum number of array elements. However, the imaging algorithm developed in the previous section is valid in the far field from the array. Using expression (2) the far field zone for the optimal 17 element array can be calculated as r≥0.5 m at 150 kHz. Therefore, increase in the number of array elements can be considered as a compromise between far-field inter-element distance and near-field array imaging.

(a) (b)

FIGURE 3. (a) Optimal 17 elements random array, circles correspond to the EMAT size; (b) effective array geometry.

(a) (b)

FIGURE 4. (a) Baseline 48 element array, circles correspond to the EMAT size; (b) effective array geometry.

In order to provide a benchmark result the 48 transducer array containing 16 transmitter elements and 32 receiver elements arranged in concentric rings with pitch circle diameters of 52 and 136 mm was chosen [4,5]. The geometry of physical array and corresponding effective array are shown in Fig.4. It can be seen that the sampling in the effective array domain is much smaller for the baseline array compared to the sparse 17 element array. For comparison the average angular spacing of the effective array elements is 2.6 ^{o} for the sparse array and 0.7^{o} for the baseline array. Note that the angular sampling calculated using expression (10) gives 5.4^{o} for the sparse array and 7.5^{o} for the baseline array.

Fig.5 presents the SNR as a function of frequency and angular position of the point reflector located in the far-field from the array. As expected the performance of the baseline array is almost omnidirectional and the performance of the sparse array slightly varies as a function of angular position of the reflector. It is seen that the performance of both arrays in terms of SNR is very similar, and the sparse array even slightly outperforms the baseline array in 140 kHz to 180 kHz frequency interval.

Fig.6 shows the SNR as a function of frequency and angular position for the point reflector located at the 0.5 m from the array center. Note that this distance corresponds to the transition zone between near and far field of the array at 150 kHz. It can be seen that the sparse array has the best SNR in the frequency range from 110 kHz to 160 kHz, where it performs slightly better than the benchmark array. However, for the frequencies higher than 160 kHz the performance of the sparse array rapidly decreases. This behavior can be explained by the fact that the boundary of the far field zone is inversely proportional to wavelength and, therefore, directly proportional to frequency. So for higher frequencies the position of the reflector becomes in the near field of the array. On the contrary, the baseline array performance doesn't deteriorate and is approximately constant between 160 kHz and 200 kHz. This is because the sampling of the baseline array is much smaller than required for the far field imaging.

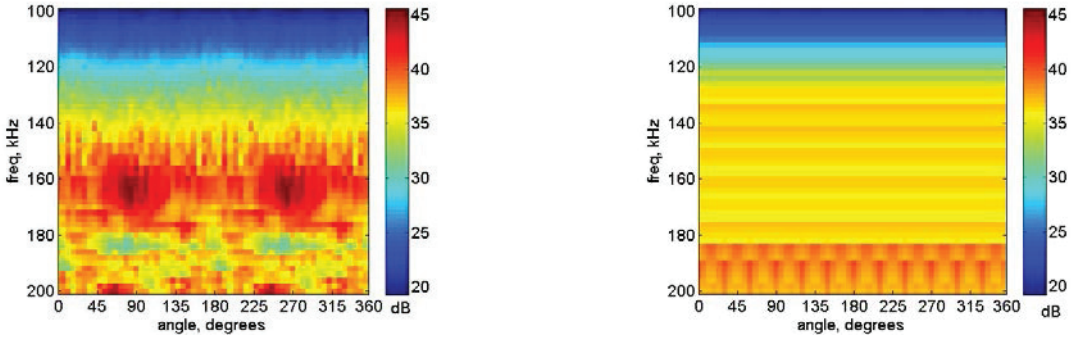

(a) (b)

FIGURE 5. SNR as a function of frequency and angular position of a point reflector located in the far-field from the array. (a) 17 element sparse array; (b) 48 element baseline array.

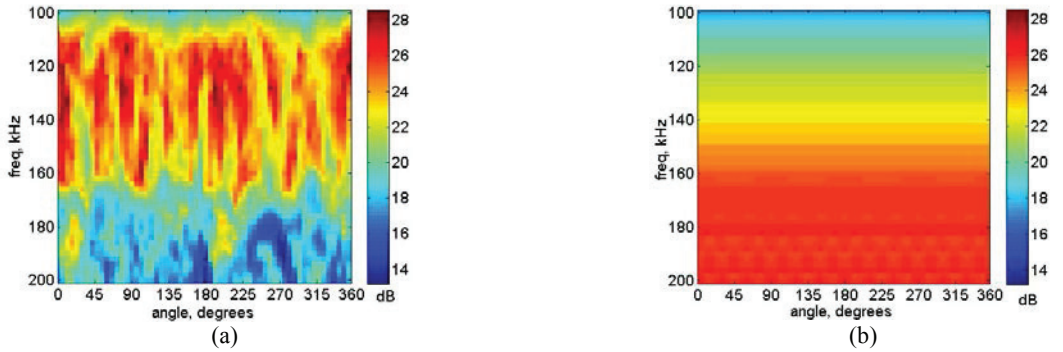

(a) (b)

FIGURE 6. SNR as a function of frequency and angular position of a point reflector located in at the 0.5m from the array. (a) 17 element sparse array; (b) 48 element baseline array.

EXPERIMENTAL RESULTS

In order to experimentally test the proposed sparse array design the full prototype has been manufactured. All experiments were conducted on a 2 m by 2 m by 3-mm-thick aluminum plate specimen containing multiple artificial defects as shown in Fig.7. The transmitted signal used was a 3 cycle Hanning windowed toneburst with a centre frequency of 150 kHz.

Firstly, a benchmark testing was performed using the 48 transducer array. One transmitter and one receiver elements were used to collect all possible 512 transmitter-receiver combinations. The result is shown in Fig.8a and it can be seen that all defects are detected. The image obtained using the sparse array is shown in Fig.8b. From the comparison with the baseline image it is seen that additional grating lobes appear at about -25dB. However, these grating lobes are caused by the nearest edge of the plate located at 0.5 m from the array. Fig.9 shows the image of the same plate, but with the sparse array shifted further away from the plate edges as illustrated in Fig.7. It is seen that all grating lobes are now below -35dB level and the performance of the sparse array is very similar to the performance of the baseline array.

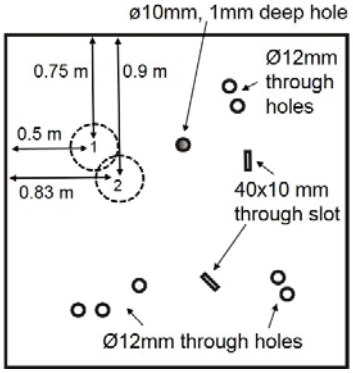

FIGURE 7. Experimental arrangement on 3-mm thick aluminum plate specimen. Dotted circles indicate the array positions.

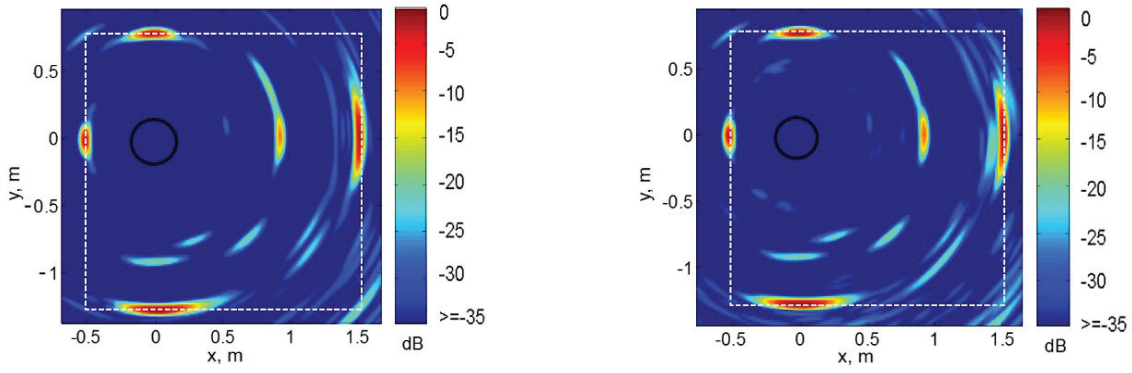

FIGURE 8. Experimental results obtained on a 3-mm-thick aluminum plate from (a) 48 element baseline array and (b) 17 element sparse array. Location of the arrays corresponds to the position 1 in Fig. 7.

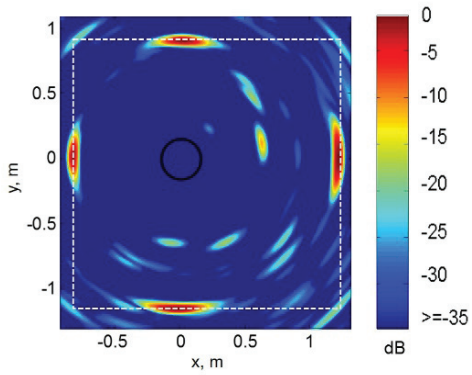

FIGURE 9. Experimental results obtained on a 3-mm-thick aluminum plate from 17 element sparse array. Location of the array corresponds to the position 2 in Fig. 7.

CONCLUSION

The general theory of the far-field imaging using transmitter-receiver guided wave array on a plate-like structure has been developed. The imaging algorithm has been formulated as an exact solution to the inverse problem. A new sampling criterion has been derived and an optimised sparse array layout has been proposed. It has been shown that the classical sampling criterion for maximum array element pitch can be significantly relaxed. A guided wave array prototype containing electromagnetic acoustic transducer elements for exciting and detecting the S_0 Lamb wave mode has been manufactured and tested on a 3-mm-thick aluminum plate with multiple artificial defects. It has been shown that the performance of the sparse array is similar to the performance of fully sampled array.

REFERENCES

1. D. E. Chimenti, "Guided waves in plates and their use in materials characterization," *Appl. Mech. Rev.*, **50**, 247–284 (1997).
2. R. T. Hoctor and S. A. Kassam, *Proceedings IEEE*, **78**, 735-752 (1990).
3. A. Velichko and P. D. Wilcox, *JASA*, **123** (1), 186-196 (2008).
4. P. D. Wilcox, *IEEE Trans. Ultrason. Ferroelectr. Freq. Contr.*, **50**, 699-709 (2003).
5. P. Wilcox, M. Lowe and P. Cawley, *IEEE Trans. Ultrason. Ferroelectr. Freq. Contr.*, **52**, 653-765 (2003).
6. P. Fromme, P. D. Wilcox, M. J. S. Lowe, and P. Cawley, *IEEE Trans. Ultrason. Ferroelectr. Freq. Contr.*, **53**, 777-785 (2006).
7. P. D. Wilcox, *IEEE Trans. Ultrason. Ferroelectr. Freq. Contr.*, **50**, 419-427 (2003).
8. A. Velichko and P.D. Wilcox, "Strategies for ultrasound imaging using two-dimensional arrays" in *Review of Progress in Quantitative Nondestructive Evaluation*, eds. D. O. Thompson and D. E. Chimenti (American Institute of Physics 1211, Melville, NY) **29**, 887 -894 (2010).